Bollettino di Geofisica Teorica ed Applicata Vol. 57, n. 4, pp. 287-300; December 2016
DOI 10.4430/bgta0183

Investigation of symmetry attribute analysis on the phase measurements of marine controlled-source electromagnetic surveys

A.H.H. Ezieke[1], A.H. Mansi[2] and G. Bernasconi[3]

[1] *Environmental and Geomatics Engineering, Politecnico di Milano, Italy*
[2] *Department of Civil and Environmental Engineering, Politecnico di Milano, Italy*
[3] *Department of Electronics, Information, and Bio-engineering, Politecnico di Milano, Italy*

(Received: March 17, 2016; accepted: October 18, 2016)

ABSTRACT In this paper we study the potential of symmetry attribute analysis applied to the phase component of electric field observations of marine controlled-source electromagnetic data. The effectiveness of symmetry attribute analysis on the phase component of marine controlled-source electromagnetic data in detecting the boundaries of resistive layer(s), such as hydrocarbon accumulation, is investigated. A comparison between symmetry attribute analysis on the phase and magnitude component of 2.5D synthetic data and a real data set is also discussed. The results presented a clear response indicative of the locations of the subsurface resistors. The phase symmetry attribute analysis proved to be effective for qualitative detection of the lateral extent of embedded resistors.

Key words: symmetry attribute analysis, controlled-source electromagnetic survey, CSEM, M-CSEM, PVO, MVO, phase and magnitude versus offset, EM.

1. Introduction

Controlled-source electromagnetic (CSEM) methods are an attractive complement or alternative to natural source soundings in some circumstances (Reynolds, 2011). They are a commonly used way of obtaining information about the electrical conductivity or resistivity of the subsurface of the Earth, and have been used in geophysical applications for many decades. Different Earth materials have resistivity across multiples of magnitude. Consequently, CSEM techniques are used to map and differentiate these materials based on that contrast. All CSEM methods utilize an active, or man-made, AC electromagnetic transmitter source to induce a secondary current in the subsurface and are an attractive complement, or alternative, to the so-called "passive-source" electromagnetic (EM) methods, such as the magneotelluric (MT), which rely on naturally occurring EM fields (Goldstein and Strangway, 1975).

In frequency-domain CSEM, the secondary current is induced by driving an alternating current at a particular frequency through a coil or a long grounded wire. This creates a primary magnetic field, which in turn induces secondary currents as it propagates through the Earth and changes with time. In time-domain CSEM, a large transmitter loop is laid out on the ground and most commonly a square-wave current is run through it. When the current abruptly goes to zero, in accordance with Faraday's law, a short-duration voltage pulse is induced in the ground, which

causes a loop of secondary currents to flow in the immediate vicinity of the transmitter wire. These secondary currents in turn create secondary magnetic and electric fields as they propagate and decay. Receivers, placed some distance away from the source, record various components of the produced EM fields. In most frequency-domain surveys, these receivers measure both the primary fields from the transmitter and secondary responses from the Earth.

CSEM methods are relatively quick in terms of collecting data, depending on the strength of the source and the desired depth of investigation, and they have been employed on land, in airborne systems and underwater (marine CSEM) for hydrocarbon exploration and detection of oil and gas (Sundberg, 1930; Constable and Srnka, 2007), in mineral prospecting (Wait, 1951), hydrological and environmental surveys (Palacky *et al.*, 1981), and in archaeology (Tite and Mullins, 1970; Osella *et al.*, 2005).

With the success of CSEM techniques in onshore mining exploration, the method was expanded into new applications for hydrocarbon exploration, initially in deep water (500 m or more) and more recently, in shallow water of less than 500 m (Peace *et al.*, 2004). The application of CSEM techniques in offshore and marine environments is termed marine controlled-source electromagnetic (M-CSEM) surveying or seabed logging, as commonly used in the industry. The basic idea behind the use of CSEM for offshore hydrocarbon exploration is to identify resistive layers in an otherwise conductive environment (Brady *et al.*, 2009).

The new M-CSEM method, although superficially similar to MT, uses an artificial electric dipole energy source instead of recording passive Earth energy, as illustrated in Fig. 1. This improves the resolution of the method by about one order of magnitude and permits the identification of thin, high-value resistors in a background matrix of low-resistivity conductor rock, down to tens of metres rather than the hundreds of metres typical of passive marine MT resolution. With offset information from, for example, a nearby discovery well, the M-CSEM method can identify a target hydrocarbon-bearing reservoir rock in a structure before it is drilled (Peace *et al.*, 2004). However, there are several methodological limitations regarding both acquisition of data and interpretation (Dell'Aversana, 2010). Intrinsic limitation of lateral and vertical resolution derive from the fact that M-CSEM is a low-frequency EM method, and in practice receivers consist of stand-alone multicomponent stations deployed on the seafloor with spacing that ranges from several hundred metres to greater than 1 km. With such sparse recording stations, good lateral resolution is difficult to provide. The method also has intrinsically low lateral resolution because of its interpretation, which is often based on the analysis of amplitude (and phase) versus offset data, observed over a large range of source-receiver distances.

Normalized anomalous amplitude response (NAR) has always been used in CSEM interpretation because it offers the advantage of a quick recognition of the anomalous electric areas and can be qualitatively correlated to causal resistive bodies at depth (Hesthammer and Stefatos, 2010). It is worth mentioning that NAR depends on the approach used for the normalization process, as well as on the model used as a reference, and normalized anomalies are generally plotted at midpoint locations between source and receiver, introducing an unavoidable spatial uncertainty. These are some of the intrinsic limitations of quantitative interpretation based on the use of NAR.

Recently, a new interpretation technique was introduced (Dell'Aversana and Zanoletti, 2008; Dell'Aversana and Zanoletti, 2010a) based on the properties of symmetry of M-CSEM data. The symmetry properties of CSEM data are easy to calculate and can be correlated with causal bodies at depth without applying any assumption of common midpoint and without any heavy

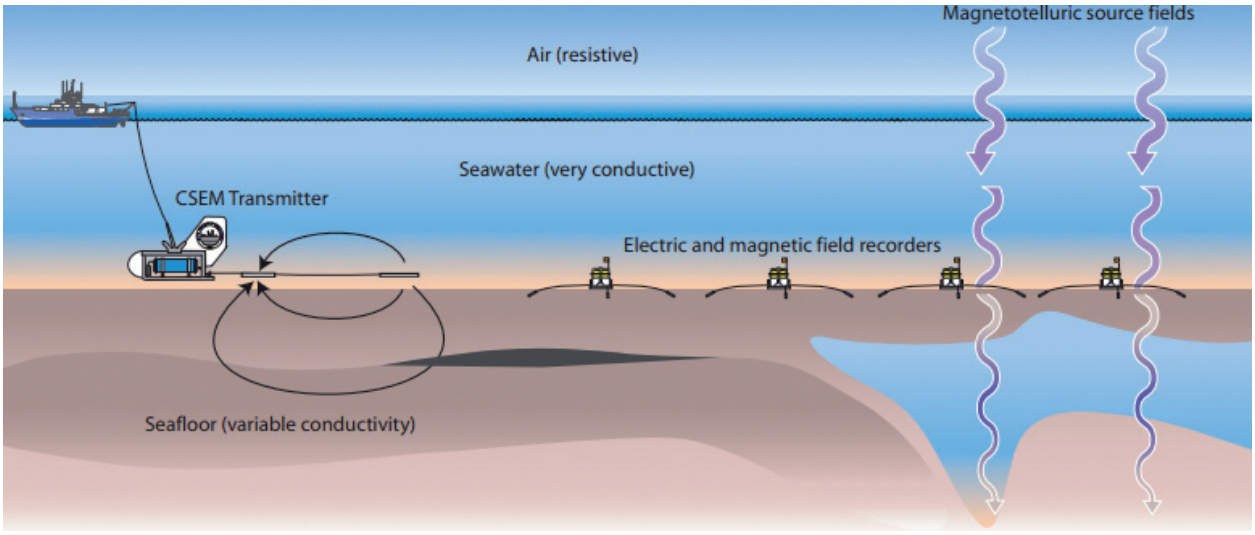

Fig. 1 - Schematic representation of the horizontal electric dipole-dipole M-CSEM method, which shows an EM transmitter being towed to the seafloor to maximize the coupling of electric and magnetic fields with seafloor rocks. These fields are recorded by instruments deployed on the seafloor at some distance from the transmitter. Seafloor instruments are also able to record magnetotelluric fields that have propagated downward through the seawater layer (source: Constable and Srnka, 2007).

modelling or inversion process. This approach, which offers the same advantages as NAR analysis, but without the intrinsic limitations of normalized amplitudes, has been demonstrated on the magnitude measurements of 3D synthetic data and on real data acquired by Eni E&P (Dell'Aversana and Zanoletti, 2010b).

In this paper, we extend the symmetry attribute analysis and its interpretation technique to phase measurements of M-CSEM data. Tests were carried out on the phase measurements of both synthetic and real data to determine the potential of obtaining relevant information that would aid in the interpretation of the M-CSEM data from the phase component of the electric field of each receiver.

Comparisons between the analysis carried out on both the magnitude and phase measurements of the electric field observation are presented. The outcome of the symmetry attribute analysis of phase measurements, when utilised with the results of the same analysis on the magnitude measurement, will significantly reduce ambiguity and risk of misleading interpretations, thus increasing the degree of certainty in decision-making.

2. Theory and synthetic tests

The signals (electric and/or magnetic field) recorded as a function of offsets at each receiver and collected in a frequency-domain seabed M-CSEM acquisition are called magnitude versus offset (MVO) and phase versus offset (PVO) plots (Eidesmo *et al.*, 2002). The attenuation trend of the measured fields versus offset depends on the resistivity distribution in the space between the source and the receiver locations, and its depth of penetration is proportional to the offset. A fundamental characteristic of M-CSEM data is the possibility to distinguish, at each receiver position, an in-towing and an out-towing part of the data that respectively corresponds to the

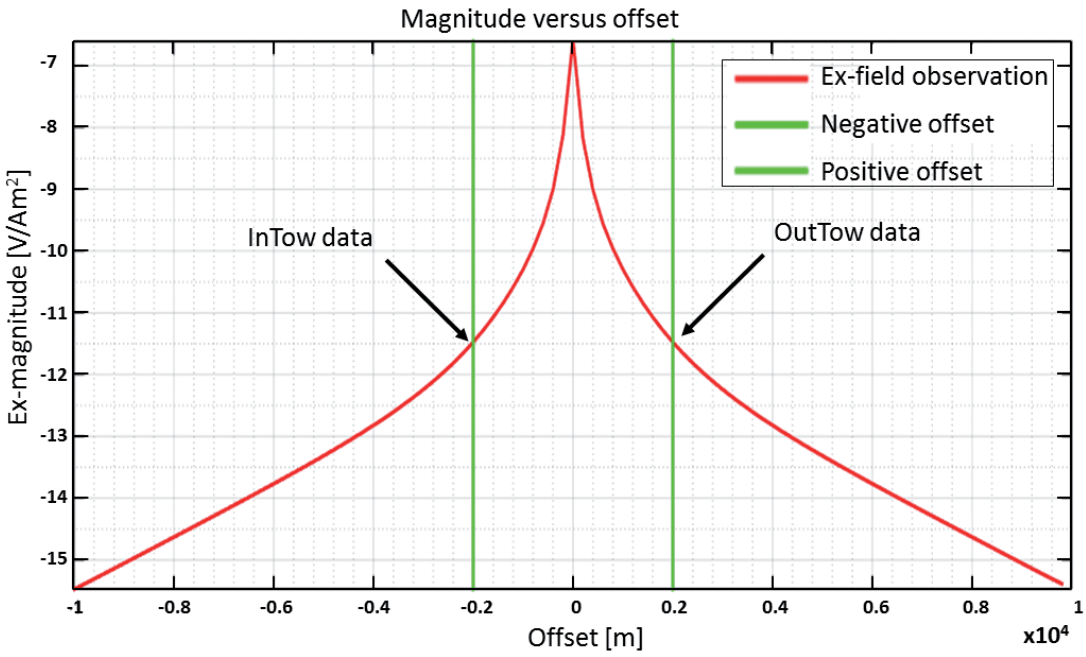

Fig. 2 - Diagrammatic representation of marine CSEM data in terms of magnitude versus offset. The two green vertical lines indicate the negative and positive offset of interest (± 2000 m in this case) with respect to zero on the horizontal, while the arrows at the point of intercept of the green lines with the represented magnitude observation indicates the in-towing and out-towing data, which corresponds, respectively, to the response recorded for decreasing source-receiver distance when the source approaches the receiver, and for increasing source receiver distances when the source is farther away from the receiver.

response recorded for the decreasing source-receiver distances and for increasing source-receiver distances, as illustrated in Fig. 2.

In the case of a half-space, uniform, or symmetrical resistivity distribution to either side of a receiver, both the MVO and PVO plots will be perfectly symmetrical with respect to the vertical axis at the receiver position, assuming flat seafloor topography. On the contrary, if a lateral resistive discontinuity exists due to a resistive body on one side of the receiver, in-towing and out-towing data will be asymmetric, and the electric (or the magnetic) response versus offset will reflect the presence of a resistive variation with different attenuation trends for the in-towing and out-towing data, respectively. The level of symmetry associated with the recorded electric and/or magnetic field at each receiver gathers as a function of offset, i.e., MVO and PVO in M-CSEM acquisition are represented by an electromagnetic attribute dubbed "Asym" (Dell'Aversana and Zanoletti, 2010a). The attribute is a unique parameter that represents a measure of asymmetry between in-towing and out-towing data and it is expected to be zero in the case of a perfect symmetry between the two sides of the receiver. On the contrary, it will have maximum absolute values above resistivity discontinuities, such that if a receiver line crosses a resistive discontinuity, the maximum asymmetry between in-towing and out-towing data will appear at the nearest receiver to the discontinuity, while the other receivers will show a progressively decreasing asymmetry for increasing distances from the lateral discontinuity.

The theory of analysis of symmetry attribute has been implemented and examined by very few authors. In the works of Gola and Bernasconi (2014), there was agreement between the results obtained using symmetry attribute analysis and their proposed method, i.e., the Pseudo-image data representation and different scaler attributes extracted from M-CSEM data. Based on the

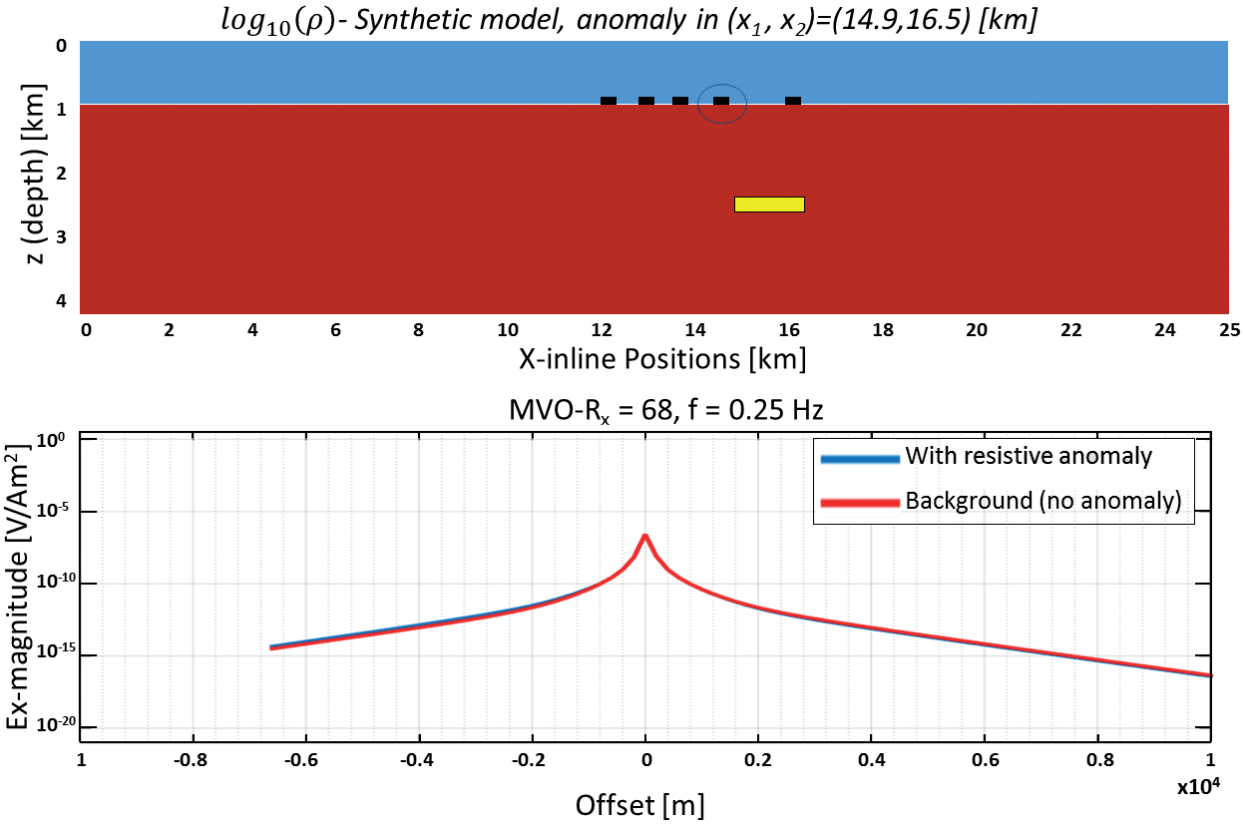

Fig. 3 - The magnitude versus offset of a receiver (RX68) at the boundary of an embedded resistive layer, in which the red and the blue curves represent the response of the uniform background (with no anomaly) and the anomalous response (with resistive anomaly) at acquisition frequency of 0.25 Hz.

results of their work, the authors concluded that the symmetry attribute analysis is very effective at estimating anomaly boundaries. However, in the scant existing literature on the theory of symmetry attribute analysis, the method has been implemented only on the magnitude component of the electric field observation of M-CSEM data. Hence, its extension to the phase component in the present work. Extensive information and details on the symmetry properties of M-CSEM data, the theory of asymmetry attribute, and principles and computations can be found in the works of Dell'Aversana and Zanoletti (2008, 2010b).

3. Test on synthetic data

The upper panel of Fig. 3 shows a simple 2.5D resistivity model consisting of a top air layer, a homogeneous half-space with resistivity (ϱ) of 1 Ω·m, and a 0.1 x 2 km resistive anomaly with ϱ of 100 Ω·m placed inside the half-space. The lower panel of Fig. 3 shows the MVO plot of one of the inline receivers (RX68) at the left boundary of the resistor with superimposed plot of the uniform background (with no anomaly) and anomalous response (with resistive anomaly) at acquisition frequency of 0.25 Hz.

The synthetic data contains electric field component (amplitude and phase) observation from a hypothesized and simulated M-CSEM acquisition. The acquisition geometry is assumed inline, with 101 transmitter and receiver gathers having a spacing of 200 m. Four different frequencies

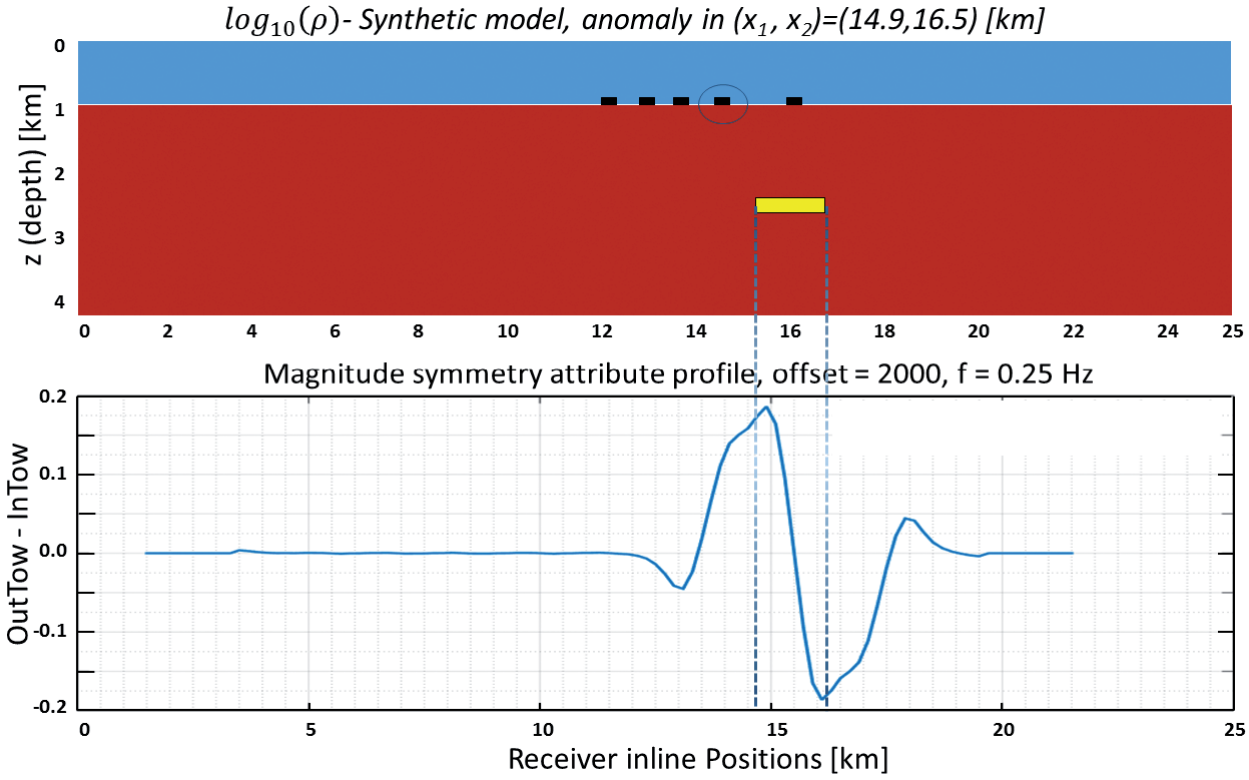

Fig. 4 - Symmetry attribute profile calculated at an offset of 2000 m and a frequency of 0.25 Hz for the magnitude component of the synthetic data. The actual maximum and minimum reflect the start and end of the resistive anomaly (yellow box) shown in the synthetic model.

were used for the data generation, i.e., 0.125, 0.25, 0.5, and 1.0 Hz, and the transmission is assumed to be from a horizontal electric dipole (HED). The highlighted receivers (black squares) are some of the 101 receivers used for the analysis, and since they are within the area of influence of the embedded resistive body, it is expected that their recorded responses should be indicative of a resistive anomaly within the subsurface.

Fig. 4 shows, in the upper panel, the same synthetic model earlier described in Fig. 3, while the lower panel shows the profile of the attribute of symmetry calculated for the inline magnitude electric response at each of the 101 receivers and for an offset of 2000 m and a frequency of 0.25 Hz (the same attribute of the symmetry was computed for the other frequencies but are not shown in this paper). In Fig. 4, there is an approximate correspondence between the boundaries of the embedded resistor (points of opposite polarity) and the absolute maxima of the asymmetry profile, indicated by the dashed blue line. Subsequently, the symmetry attribute analysis is extended to the phase measurement of the synthetic data, in order to determine if there is a correspondence of them with the result of the analysis on the magnitude.

Fig. 5 shows, in the bottom panel, the PVO plot of RX68 (same receiver considered for the MVO analysis) with the superimposed plots of the uniform background (with no anomaly) and anomalous response (with resistive anomaly) at acquisition frequency of 0.25 Hz. The upper represents panel the synthetic model described earlier in Fig. 3. From the PVO plot, the anomalous response (blue curve) overlapping the uniform background (red curve) is indicative of the presence of a possible embedded resistive body within that area of the subsurface.

Generally, in a real scenario, the varying trend of the measured phase usually indicates the

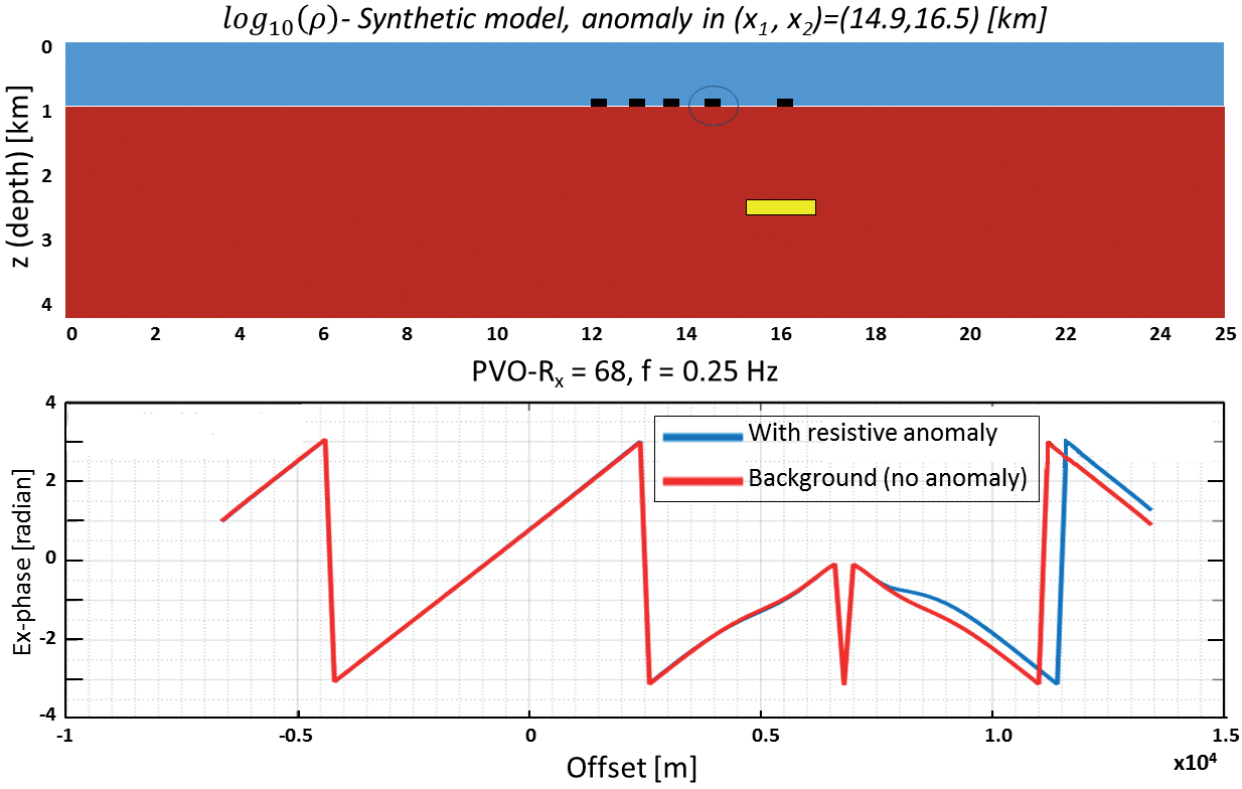

Fig. 5 - The phase versus offset plot of the receiver 68 (RX68) computed at a frequency of 0.25 Hz shows the effect of the presence of a resistive anomaly.

presence of noise in the information carried by the transmitting phase, and there is therefore a need to unwrap the phase and obtain a physically continuous phase. Generally, phase unwrapping retrieves the correct phase from the modulo -2π measured phase, which overcomes the discontinuity of the measured values ranging from [-π, π] (Ching *et al.*, 1992). Phase aliasing and phase jump are the main problems encountered in phase signal processing, however, because by applying phase unwrapping, the measured phase signal is altered (Fornaro *et al.*, 1996). The first is caused by an insufficient sampling rate, defined by the Nyquist rate, while the latter occurs when the phase difference of two adjoining pixels exceeds the magnitude of 2π, resulting in a discontinuity (Huntley, 1989). The works of Ghiglia *et al.* (1987), Lin *et al.* (1994), Pritt (1996), and Ghiglia and Pritt (1998) present several proposed solutions for tackling error propagation and integration in phase measurements.

In the present work, the simple and straightforward one-dimensional (1D) phase unwrapping is implemented. This involves detection of the positions of the discontinuities, or phase jumps, through evaluation of the derivative of the phase measurements with respect to the inline position axis, which is essentially continuous, except for the presence of spikes of 2π amplitude at certain points. Fig. 6 shows on the right the original wrapped phase of the electric field, and on the left is the phase map obtained after unwrapping the phase component of the electric field observation (in red) at a specified offset of interest indicated by the green parallel lines.

The practicality of the phase unwrapping cannot be duly understood from application to the phase measurement of the synthetic data, which is synthetic and expected to be devoid of noise. Contrary to what is obtainable from perfect synthetic data, the noticeable discrepancy in the plot

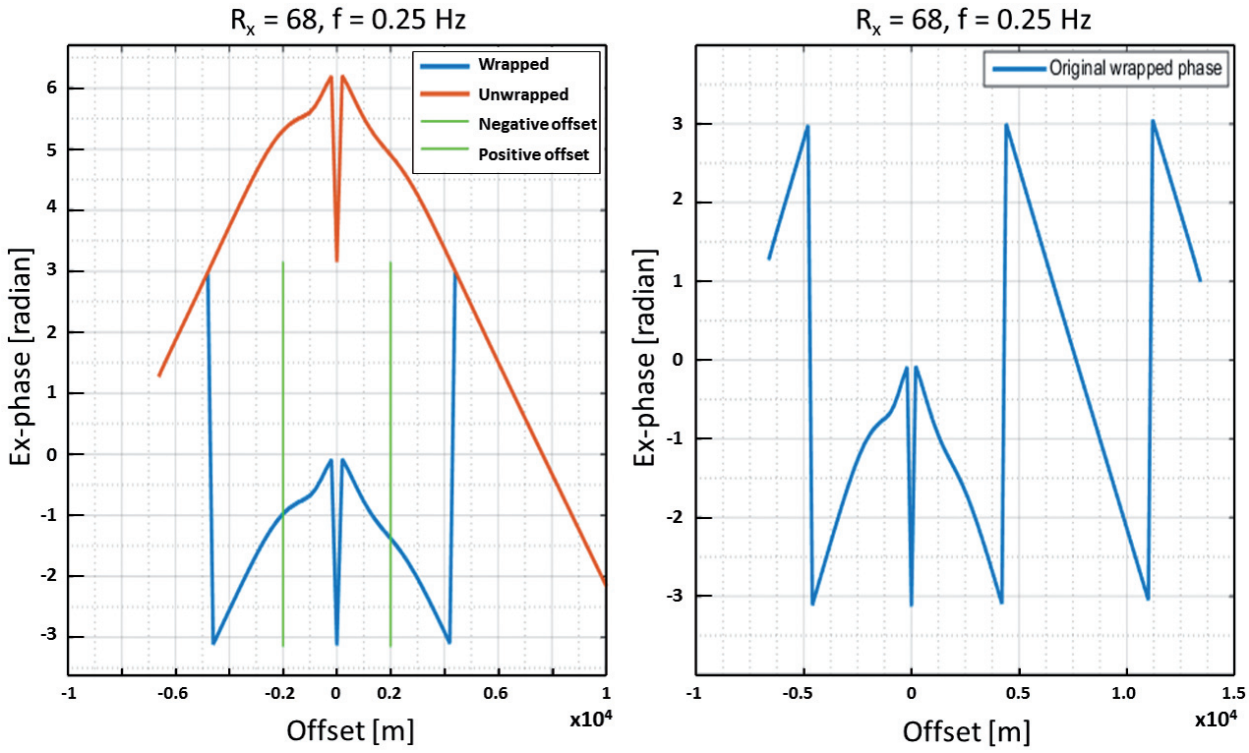

Fig. 6 - The left panel represents the results of the synthetic data phase unwrapping up to a maximum offset of 10000 m, and the right panel represents a part of the original wrapped phase measured by receiver (RX68) at a maximum offset of 15000 m.

of Fig. 6 (red plot) is due to error in the model used for the synthetic data generation. However, this error is clipped off at an offset of 2000 m, so as to obtain the phase with reliable information. Fig. 7 shows, in the bottom panel, the asymmetry attribute response of the same frequency and offset (0.25 Hz and 2000 m offset) as that computed on the magnitude, and in the top panel is the synthetic model with single anomaly.

From Fig. 7, it is possible to appreciate how the boundaries of the resistive anomaly show a relatively good correspondence with the picks of the symmetry attribute profile, as indicated by the dashed blue line.

4. Test on Gulf of Mexico data

The Gulf of Mexico (GOM) benchmark data set is a real data set, with a file format corresponding to that used by Scripps Institution of Oceanography and made available by Chevron Corporation. The data contain electric field component (amplitude and phase) observations from both M-CSEM surveys and marine magnetotelluric acquisition. The acquisition was done with 51 transmitters and 381 receivers with a spacing of 1500 m. Five M-CSEM frequencies (0.06, 0.18, 0.25, 1.25, and 2.25 Hz) were used for the acquisition, but for this paper, the frequency of 0.06 Hz and three different offsets (2000, 3000, and 4000 m) are emphasized.

Due to the unavailability of the true model of the GOM benchmark, there was a need to understand if the trend in the computed symmetry attribute of this data is a result of resistive anomalies or other factors such as airwave effects or ocean-induced fields. Therefore, we simulated

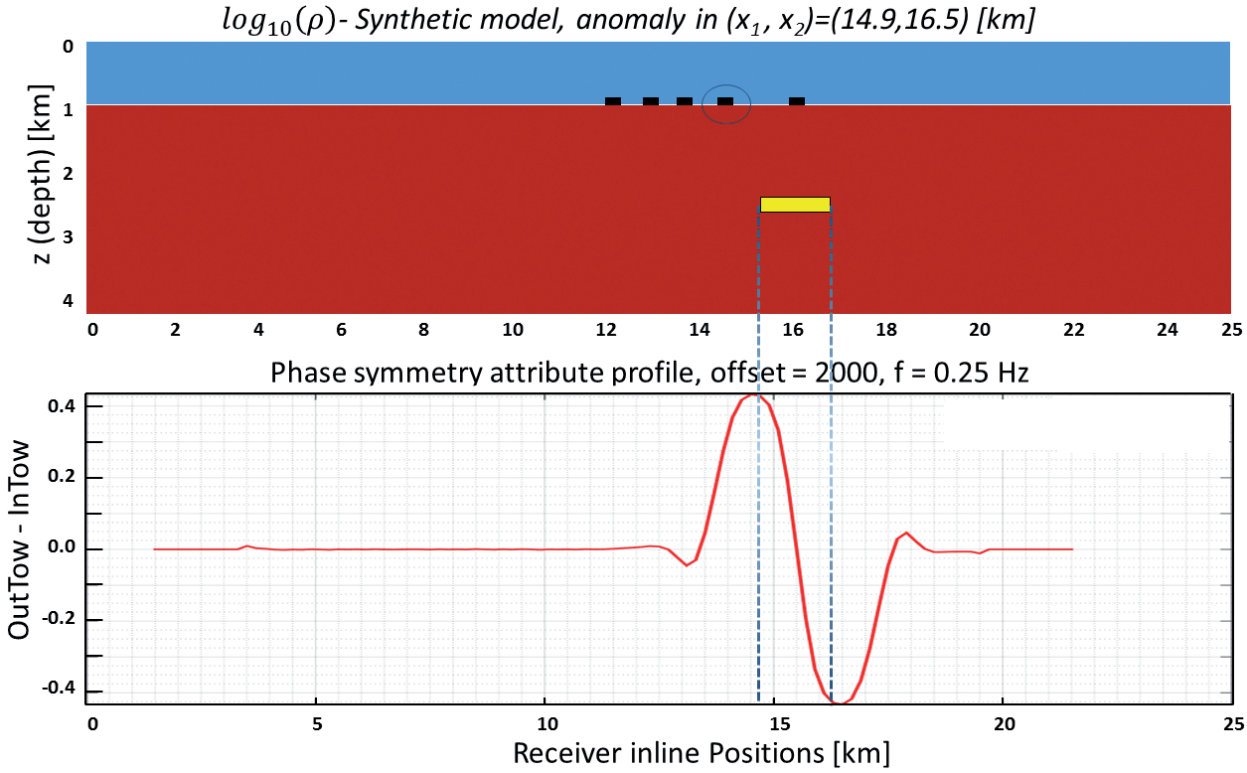

Fig. 7 - Symmetry attribute profile computed at an offset of 2000 m and frequency of 0.25 Hz for the phase component of the synthetic data. The actual maximum and minimum of the profile reflect the start and end of the resistive anomaly (yellow box) shown in the synthetic model.

the seabed bathymetry, which is one of the biggest factors affecting detectability in M-CSEM survey. The top panel of Fig. 8 reports the simulated seafloor-towed transmitters (black line), and the receivers' trajectory (blue line), which coincides with the bathymetry of the seabed (cyan line). The idea behind including the seabed bathymetry is that it represents reality to a reasonable level, and it is expected that in a situation where the trend is caused by the sea bottom inhomogeneity, a comparison of the trends of the symmetry attribute profile and the bathymetry will show an approximate match. Otherwise, the difference between the trends will be evident, indicating that something in the subsurface, most probably a resistive anomaly, contributes or causes the noticeable difference. Fig. 8 shows, in the top panel, the simulated GOM data bathymetry, and in the bottom panel the symmetry attribute profile at a frequency of 0.06 Hz and offsets of 2000, 3000, and 4000 m.

As shown in Fig. 8, the outcome of the comparison is an understanding that resistive anomalies probably do exist in the subsurface, and are the main reason for the response of the symmetry attribute profile. Based on this finding and the principle of interpretation of the symmetry attribute profiles, i.e., maxima and minima of the symmetry response, the model showing the positions of the resistors was produced. Fig. 9 shows, in the top panel, the symmetry attribute response at a frequency of 0.06 Hz and offsets of 2000, 3000, and 4000 m. In the bottom panel are shown a simulated image of the sea (in blue), the bathymetry, the unknown model (in red with a question mark) and the proposed resistors (yellow rectangles). It is expected that the true model will have at least five resistors/resistive anomalies at different depths and positions in the subsurface. The symmetry attribute analysis is extended to the phase measurement of the GOM data, and our earlier

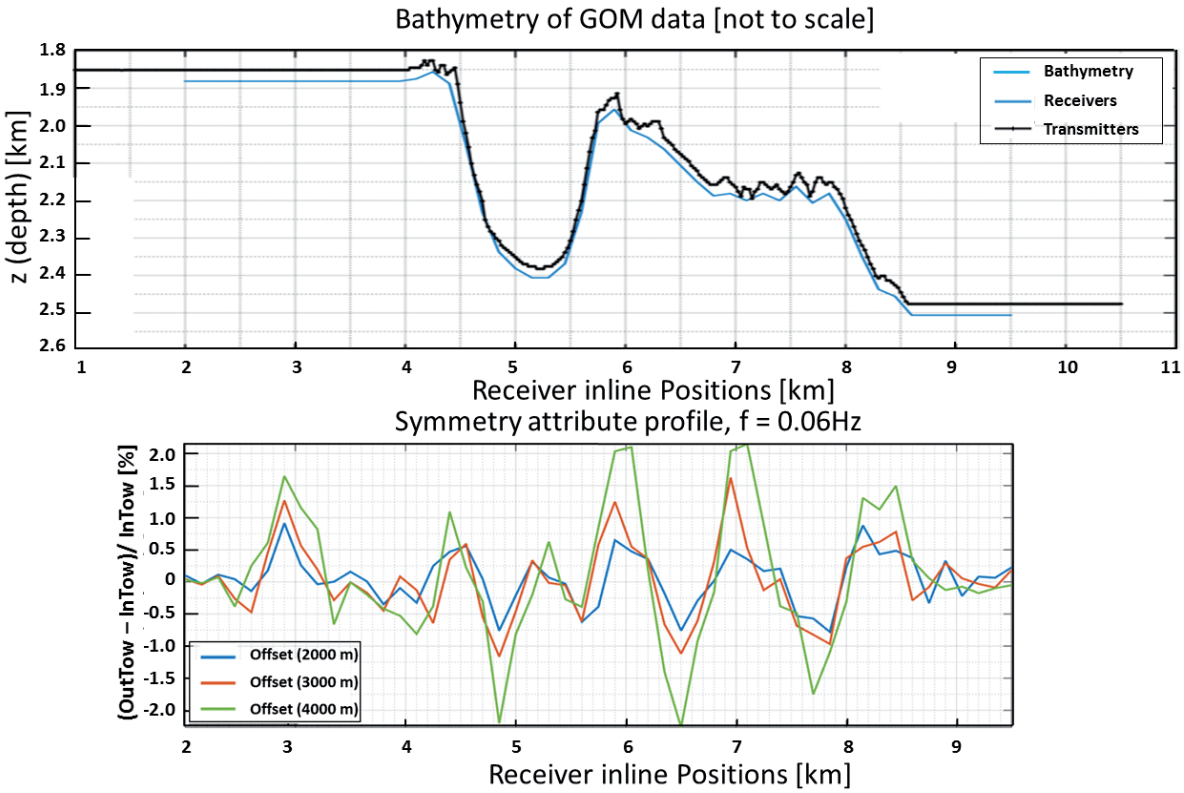

Fig. 8 - The bathymetry and symmetry attribute response for the Gulf of Mexico data set, where the top panel shows the bathymetry (seafloor) of the GOM seabed (cyan line), the simulated receivers' locations (blue line), and the simulated seafloor-towed transmitters (black line). The bottom panel illustrates the symmetry attribute response at an acquisition frequency of 0.06 Hz for different offset values (i.e., 2000, 3000, and 4000 m).

projections about the possible positions and number of the embedded resistors is reconfirmed. To obtain phase measurements with reliable information and devoid of noise, the phase is unwrapped, thereby compensating for the numerous attenuations and jumps in the original extracted phase. An arbitrary starting point of mutilation at offset of 1000 m is defined in the phase map, and the physical continuous phase variation is reconstructed by the addition of positive pi ($+\pi$) when both in-towing and out-towing data are negative, and a negative pi ($-\pi$) when the in-towing and out-towing data are positive.

The outcome of unwrapping the phase formed the basis for the implementation of the symmetry attribute analysis on the phase measurements. Fig. 10 shows, on the right, the original wrapped phase of the electric field, and on the left is the phase map obtained after unwrapping the original phase (in red, above), and part of the original phase before unwrapping (in blue, below). The parallel green lines indicate the offset at which the phase is unwrapped (in this case 1000 m) in which the short offsets that represent the mixed-phase and the direct arrivals have been muted by setting them to a constant value equivalent to the measured phase at the zero offset.

Subsequently, the symmetry attribute is computed on the unwrapped phase of the GOM data at a frequency of 0.06 Hz and offsets of 2000, 3000, and 4000 m, and the obtained symmetry profile is compared to that obtained from the magnitude of the electric field. Fig. 11 shows, in the top panel, the symmetry attribute profile of the phase measurements, while in the bottom panel is the symmetry attribute profile of the magnitude measurements.

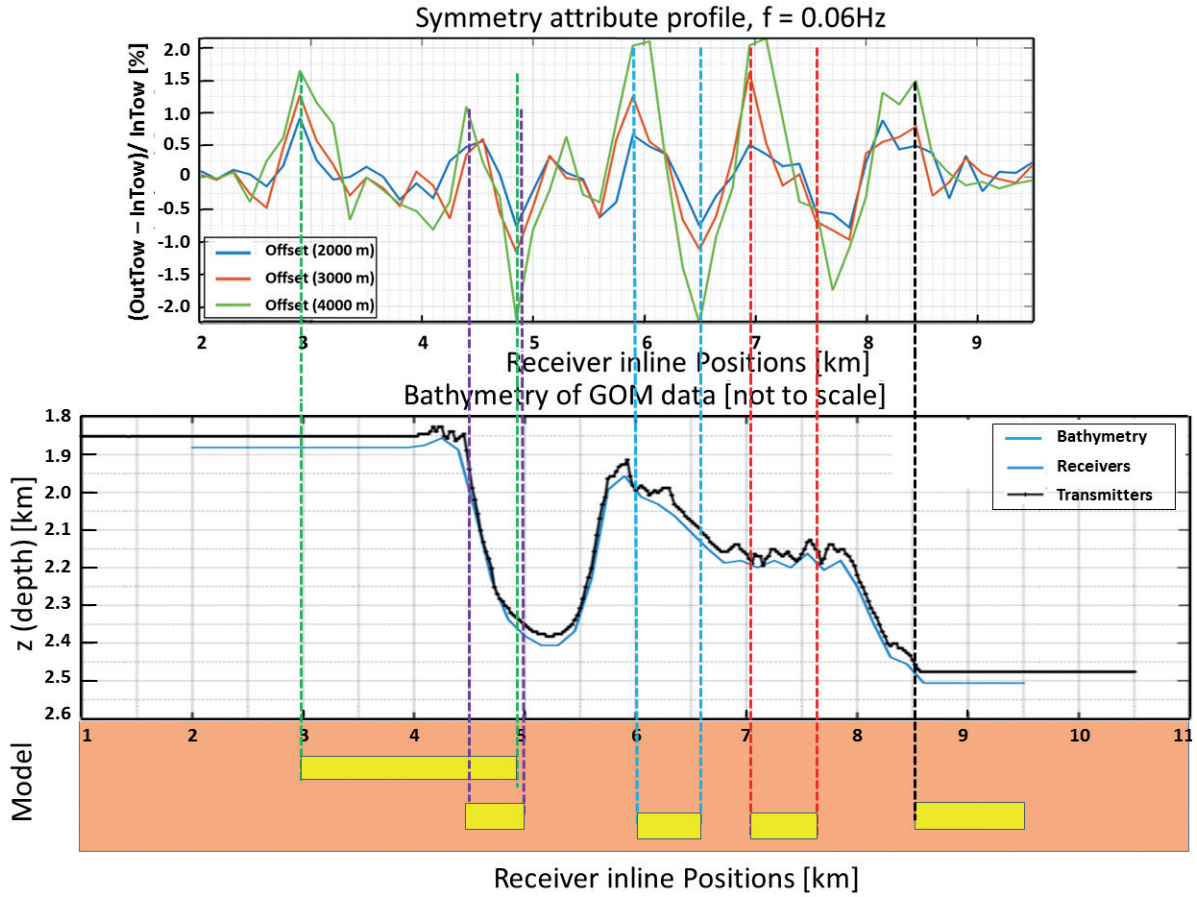

Fig. 9 - The simulated model of the GOM data set based on the magnitude symmetry attribute profile.

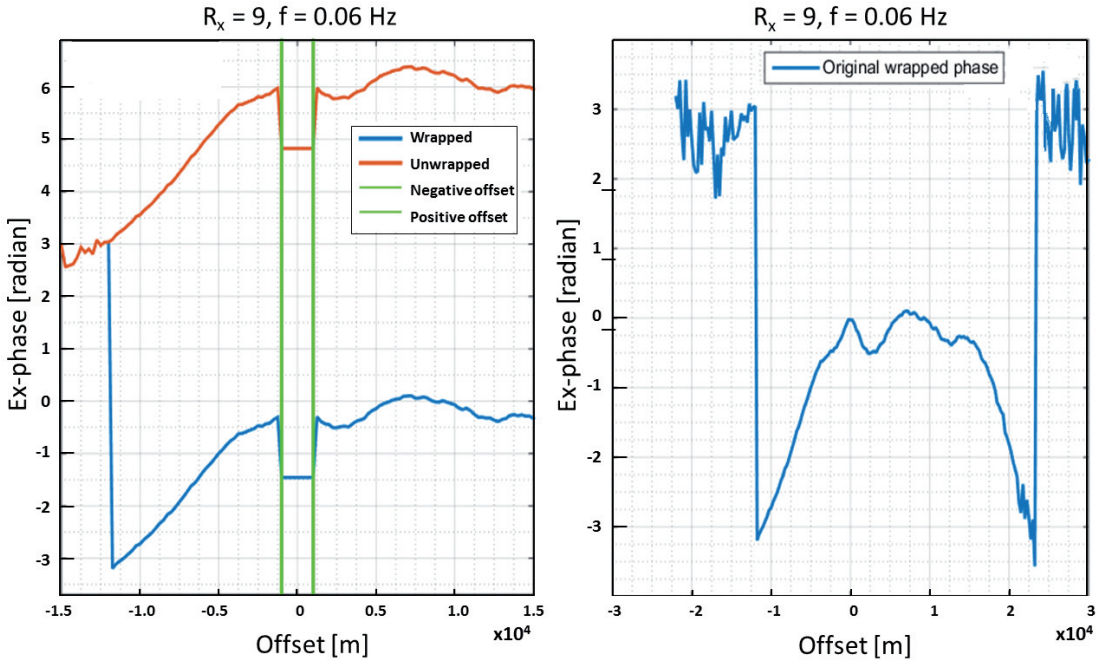

Fig. 10 - GOM phase measurement unwrapping, where the left panel represents the results of the data phase unwrapping up to a maximum offset of 15000 m, and the right panel represents a part of the original wrapped phase measured by a receiver (RX9) at an acquisition frequency of 0.06 Hz and a maximum offset of 30000 m.

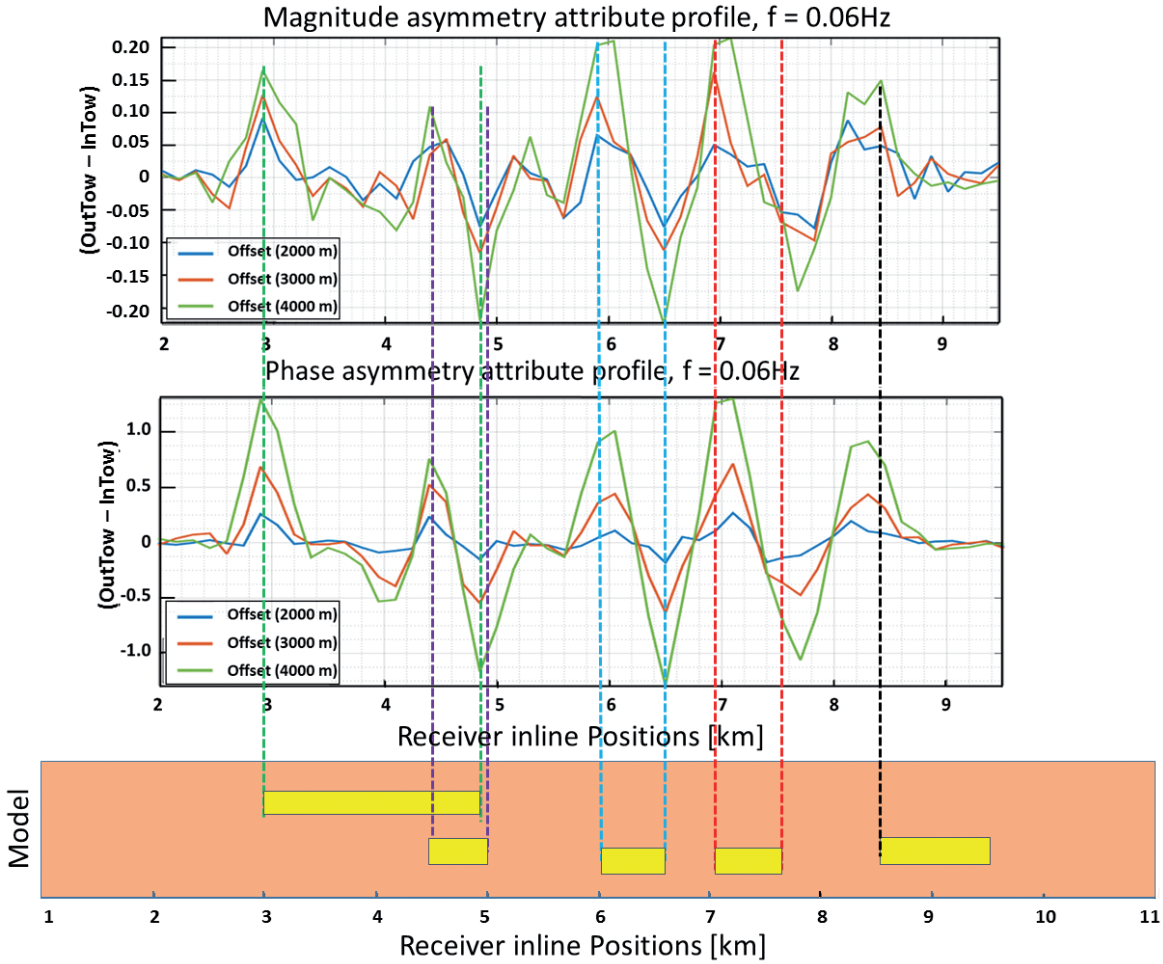

Fig. 11 - Simulated model of the GOM data set based on the comparison between the phase and magnitude symmetry attribute profiles at an acquisition frequency of 0.06 Hz and offset values of 2000, 3000, and 4000 m, respectively.

In Fig. 11, it can be seen that both the phase and magnitude symmetry attribute profiles are qualitatively similar, revealing approximately corresponding results that suggest at least five resistive anomalies (yellow rectangles) at different depths and positions. The unavailability of the GOM true resistivity model limits the interpretation of the symmetry profiles. However, Dell'Aversana and Zanoletti (2008), who introduced the concept of the symmetry attribute method using the magnitude component of M-CSEM, provided the following proven principles for interpretation of the results obtained from implementation of this EM attribute:

- asymmetry increases when approaching reservoir boundaries;
- the asymmetry has opposite polarity for the two opposite boundaries of the same resistor;
- minimum asymmetry appears above the centre of the resistor or away from the resistor at distances from its boundaries;
- asymmetry due to deep resistors is highlighted at low frequencies and long offsets;
- the offset where the maximum asymmetry appears is directly proportional to the resistor depth, and also depends on the background resistivity.

The authors proved the effectiveness of this interpretation approach through demonstration of the magnitude component of 3D synthetic data and on real data, considering different frequencies and at both short and long offsets.

The aforementioned principles are the bases on which the results of the analysis of the phase component of GOM data carried out in this paper are interpreted. In Fig. 11, it can be seen that the positions of the suggested resistive anomalies approximately coincide with the positions of the actual and local maxima and minima of the attribute. However, the results (the suggested resistive anomalies) presented in this paper are for symmetry attribute calculated at a single low frequency of 0.06 Hz and relatively short offsets of 2000, 3000, and 4000 m, so it is expected that at other frequencies (low to high) and longer offset, more resistive anomalies (shallow and deep) could be detected. Furthermore, the comparison between the symmetry attribute calculated on the magnitude and phase component of the GOM data set, presented in Fig. 11, shows a qualitative congruence, with maxima and minima of the attribute in the same positions and revealing the same possible locations of resistive anomalies and number of resistors.

5. Conclusions

We have extended the concept of symmetry attribute analysis to the phase component of the M-CSEM data set and have presented a comparative result with the attribute calculated using the magnitude measurements of a synthetic and a real M-CSEM case study. The results of the synthetic test show that the analysis of the phase symmetry attribute is able to detect and delineate the lateral extent of resistive layers.

In the analysis of the real Gulf of Mexico M-CSEM data set, the inferred positions and the lateral locations of the resistive discontinuities are considered to be geologically meaningful, based on the proven interpretation methodology for symmetry attribute provided in the literature. The symmetry attribute analysis can autonomously provide a quick preliminary model of the resistivity discontinuities. For refined results, M-CSEM data must be integrated with other geophysical data (e.g., seismic and/or MT). Moreover, it should be mentioned that the symmetry attribute analysis, for both the magnitude and the phase components, cannot replace modelling and joint inversion. Rather, the symmetry properties can provide constraints to speed up the inversion. Finally, the joint utilisation of the symmetry attribute calculated on the phase and magnitude components will be effective for the interpretation of M-CSEM data, and will increase the degree of certainty in making decisions about exploration prospects.

Acknowledgements. The authors would like to thank Chevron Corporation for making publicly available the GOM benchmark data set and for the authorization to use it for this study.

REFERENCES

Brady J., Campbell T., Fenwick A., Ganz M., Sandberg S.K., Buonora M.P.P., Rodrigues L.F., Campbell C., Combee L., Ferster A. and Umbach K.E.; 2009: *Electromagnetic sounding for hydrocarbons*. Oilfield Rev., **21**, 4-19.

Ching N., Rosenfeld D. and Braun M.; 1992: *Two-dimensional phase unwrapping using a minimum spanning tree algorithm*. IEEE Trans. Image Process., **1**, 355-365, <http://ieeexplore.ieee.org/document/148608/?arnumber=148608>, doi:10.1109/83.148608.

Constable S. and Srnka L.; 2007: *An introduction to marine controlled-source electromagnetic methods for hydrocarbon exploration*. Geophys., **72**, WA3-WA12, doi:10.1190/1.2432483.

Dell'Aversana P.; 2010: *Accurate detection of resistivity anomalies using the symmetry attribute and inversion of marine CSEM data*. The Leading Edge, **29**, 662-669.

Dell'Aversana P. and Zanoletti F.; 2008: *Accurate detection of reservoir boundaries using electromagnetic attributes and inversion of marine CSEM data*. In: Extended abstract, 70th EAGE Conference and Exhibition, Roma, Italy, doi:10.3997/2214-4609.20147710.

Dell'Aversana P. and Zanoletti F.; 2010a: *Multi-frequency symmetry analysis of marine CSEM data for separating the effects of multiple resistors*. In: Proc. EMG International workshop, Capri, Italy.

Dell'Aversana P. and Zanoletti F.; 2010b: *Spectral analysis of marine CSEM data symmetry*. First Break, **28**, 43-51.

Eidesmo, T., Ellingsrud S., MacGregor L.M., Constable S., Sinha M.C., Johansen S.E., Kong F.N. and Westerdahl H.; 2002: *Sea Bed Logging (SBL), a new method for remote and direct identification of hydrocarbon filled layers in deepwater areas*. First Break, **20**, 144-152.

Fornaro G., Franceschetti G. and Lanari R.; 1996: *Interferometric SAR phase unwrapping using Green's formulation*. IEEE Trans. Geosci. Remote Sens., **34**, 720-727, <http://ieeexplore.ieee.org/document/499751/?arnumber=499751>, doi:10.1109/36.499751.

Ghiglia D.C. and Pritt M.D.; 1998: *Two-dimensional phase unwrapping: theory, algorithms, and software*. John Wiley and Sons, Inc., New York, NY, USA, 512 pp.

Ghiglia D., Mastin G. and Romer O.L.; 1987: *Cellular-automata method for phase unwrapping*. J. Opt. Soc. Am., **4**, 267-280, <https://www.osapublishing.org/josaa/fulltext.cfm?uri=josaa-4-1-267&id=2636>, doi:10.1364/JOSAA.4.000267.

Gola A. and Bernasconi G.; 2014: *Quick qualitative CSEM data interpretation*. In: Proc., 84th Annual Meeting, Soc. Explor. Geophys., Denver, CO, USA, pp. 813-817, <http://dx.doi.org/10.1190/segam2014-1674.1>, doi:10.1190/segam2014-1674.1.

Goldstein M.A. and Strangway D.W.; 1975: *Audio-frequency magnetotellurics with a grounded electric dipole source*. Geophys., **40**, 669-683, <http://dx.doi.org/10.1190/1.1440558>, doi:10.1190/1.1440558.

Hesthammer J. and Stefatos A.; 2010: *The performance of CSEM as a de-risking tool in oil and gas exploration*. In: Expanded Abstracts, 29th Technical Program, Soc. Explor. Geophys., Denver, CO, USA, pp. 675-679, <http://dx.doi.org/10.1190/1.3513873>, doi:10.1190/1.3513873.

Huntley J.M.; 1989: *Noise-immune phase unwrapping algorithm*. Appl. Opt., **28**, 3268-3270, <https://www.osapublishing.org/ao/fulltext.cfm?uri=ao-28-16-3268&id=32669>, doi:10.1364/AO.28.003268.

Lin Q., Vesecly J.F. and Zebeker H.A.; 1994: *Comparison of elevation derived from INSAR data with DEM over large relief terrain*. Int. J. Remote Sens., **15**, 1775-1790, <http://www.tandfonline.com/doi/abs/10.1080/01431169408954208>, doi:10.1080/01431169408954208.

Osella A., Vega M. and Lascano E.; 2005: *3D electrical imaging of an archaeological site using electrical and electromagnetic methods*. Geophys., **70**, G101-G107, doi:10.1190/1.1993727.

Palacky G., Ritsema I. and Jong S.; 1981: *Electromagnetic prospecting for groundwater in Precambrian terrains in the Republic of Upper Volta*. Geophys. Prospect., **29**, 932-955, doi:10.1111/j.1365-2478.1981.tb01036.x.

Peace D., Meaux D., Johnson M. and Taylor A.; 2004: *Controlled-source electromagnetics for hydrocarbon exploration*. Houston Geol. Soc. Bull., **47**, 31-45.

Pritt M.D.; 1996: *Phase unwrapping by means of multigrid techniques for interferometric SAR*. IEEE Trans. Geosci. Remote Sens., **34**, 728-738, <http://ieeexplore.ieee.org/document/499752/?arnumber=499752&tag=1>, doi:10.1109/36.499752.

Reynolds J.M.; 2011: *An introduction to applied and environmental geophysics, 2nd ed*. John Wiley and Sons, Inc., New York, NY, USA, 710 pp.

Sundberg K.; 1930: *Electrical prospecting for oil structure*. AAPG Bull., **14**, 1145-1163, <http://archives.datapages.com/data/bulletns/1917-30/data/pg/0014/0009/1100/1145.htm>.

Tite M. and Mullins C.; 1970: *Electromagnetic prospecting on archaeological sites using a soil conductivity meter*. Archaeom., **12**, 97-104, doi:10.1111/j.1475-4754.1970.tb00010.x.

Wait J.; 1951: *A conducting sphere in a time varying magnetic field*. Geophys., **16**, 666-672, doi:10.1190/1.1437716.

Corresponding author: Ahmed H. Mansi
Department of Civil and Environmental Engineering, Politecnico di Milano
Piazza Leonardo da Vinci 32, 20133 Milano, Italy
Phone: +39 02 2399 6530; fax: +39 02 2399 2206; email: ahmed.hamdi@polimi.it